Adv. Theor. Appl. Mech., Vol. 2, 2009, no. 2, 75 - 92

Application of a Perfectly Matched Layer Boundary Condition to Finite Element Modeling of Elastic Wave Scattering in Cracked Plates

Abdel-Rahman Mahmoud[1] and Yunhua Luo[2]

Department of Mechanical & Manufacturing Engineering
University of Manitoba, Winnipeg MB R3T 5V6
[1]AMahmoud6@slb.com, [2]luoy@cc.umanitoba.ca

Abstract

This paper investigates the applicability of a displacement-based, Finite Element (FE) implementation of a time-domain, split-field Perfectly Matched Layer (PML) formulation to numerical modeling of elastic, Pressure, Shear-Vertical (P-SV) wave propagation and scattering in infinite plates for the purpose of crack characterization. Results obtained using the proposed model satisfy reciprocity and closely agrees with available analytical and semi-analytical solutions. Results obtained through FE-PML modeling of forward scattering by cracks confirm previous experimental findings and can potentially help optimizing experimental parameters.

Keywords: perfectly matched layer, finite element modeling, elastic waves, plates

1 Introduction

Plates and plate-like members are widely utilized in civil infrastructures. They may develop cracks as a result of overloading or environmental adversities. Guided elastic waves can be used to characterize these cracks to decide if a replacement or a repair is needed. Mathematical modeling of the interaction of guided elastic waves with a crack is an integral part of such characterization. Due to inherent irregularity of a crack, a numerical method is usually required to solve the governing equations of wave propagation. Available numerical methods include the finite difference method

(FDM), finite element method (FEM), boundary element method (BEM), etc. Among them, the finite element method is the most popular one, due to its amenability to implementation and its adaptability to complex geometry.

A plate's thickness is usually much smaller that the other two dimensions. Therefore, in studying wave propagation in plates, it is reasonable to assume that a plate is infinite in the two dimensions other than its thickness. This assumption is convenient for constructing analytical solutions; however, it is inconvenient for finite element implementation. An easy but computationally expensive solution to this dilemma is to shift numerical reflections outside a desired time window by laterally extending the finite element mesh. However, an economical alternative is to use absorbing boundary conditions or layers. An absorbing layer interfacing with the domain boundary that does not return any reflection at any frequency or angle of incidence was introduced by Berenger [1] in the context of computational electromagnetics to solve Maxwell's equation, using a Finite Difference Time-Domain method (FDTD). This absorbing layer became well-known in the literature as the Perfectly Matched Layer (PML).

Chew and Weedon [2] interpreted the PML as a complex coordinate stretching. This interpretation widely inspired researchers to apply the PML to other disciplines. Hastings et al. [3], for example, introduced the PML to elastic P-SV wave propagation in an infinite medium. They employed the FDTD method to formulate a PML for the stress-velocity equations in the form of compressional and shear potentials. Chew and Liu [4] showed the feasibility and stability of PML solutions for two-dimensional (2D) and three-dimensional (3D) stress-velocity, elastodynamic equations in isotropic elastic media. Liu [5] formulated PMLs for elastic wave propagation in polar and cylindrical coordinates. He introduced integral complex coordinate stretching to keep the number of unknowns in the formulation the same as that for Cartesian coordinates. Collino and Tsogka [6] applied the PML to a linear elastodynamic problem in anisotropic heterogeneous media using the FDTD. Becache et al. [7] used the PML with a fictitious-domain, mixed FEA instead of FDTD to overcome the inadequacy of the latter for irregular geometries. Komatitsch and Tromp [8] used wave-equation splitting to introduce a time-domain, spectral-element formulation of the PML boundary condition for the second-order, seismic wave equation. Their formulation is amenable to explicit time integration. Basu and Chopra [9, 10] have reported both steady-state and time-domain FE-PML formulations for 2D elastodynamic problems in an infinite layer resting on a semi-infinite elastic media. The time-domain formulation in [10] was obtained without field-splitting through transforming steady-state equations by a special choice of coordinate stretching functions. The time integration in [10] was implicit and a system of equations was solved at each time step. Just recently, Basu [11] has extended his work in [10] to 3D and made it amenable to explicit time integration by lumping inertial matrices inside the PML.

This paper explores the use of a split-field PML in FE modeling of elastic, P-SV wave propagation and scattering in infinite plates. An FE-PML model consists of a truncated plate surrounded by two PMLs on each side. Frequency-domain equations of the PML model are obtained from its counterpart in the infinite plate by complex coordinate stretching. Displacement wave field in the resulting frequency-domain equation is split

into four components in order to facilitate inverse transformation into time domain. A Galerkin method is, then, followed to cast the time-domain governing equations into finite element equations. A step-by-step scheme to march through discrete times inside the PML region is given.

The motivation behind this work is to show: 1) accuracy and cost-effectiveness of an FE-PML model compared to a full FE idealization; 2) application of FE-PML modeling to parametric studies of elastic wave interaction with defects. Reciprocity check and comparison with literature data establish the validity of FE-PML modeling. An FE-PML model consumes considerably lower CPU time than an equivalent full FE model, making it cost-effective. Numerical examples are presented to demonstrate potential uses of the FE-PML approach in numerical modeling of 2D elastic wave interaction with cracks and delaminations.

2 Finite element model of perfectly matched layers

The subject of the current study is an infinitely-long plate having a uniform thickness, H, with and without a crack. The plate is described using a rectangular coordinate system. The origin is located on the bottom surface of the plate as shown in Fig. 1. The physical domain of the problem, Ω^{∞}, is a planar x-z cross-section. The plate is excited by a line load, p. A crack perpendicular to the x-z plane can be described by its tip coordinates, (x_c, z_c), its length, l_c, and the counter-clockwise angle, α, that the crack makes with x-axis. Coordinates, (x, z), corresponding displacements, (u, w), and crack length, l_c, are divided by plate's thickness, H, to get their dimensionless counterparts $(\bar{x}, \bar{z})$, $(\bar{u}, \bar{w})$, and $\bar{l}_C$. This implies a dimensionless thickness $\bar{H} = 1$. Dimensionless elastic constants, $\bar{c}_{ij}$, stress, $\bar{\sigma}$, line load, $\bar{p}$, density, $\bar{\rho}$, frequency, $\bar{\omega}$, time, $\bar{t}$, shear-wave speed, $\bar{c}_s$ are related to their dimensional counterparts by:

$$\begin{aligned} &\bar{c}_{55}=1;\ \bar{c}_{ij} = \frac{c_{ij}}{c_{55}}:\ (i, j = 1,2);\ \bar{\sigma} = \frac{\sigma}{c_{55}};\ \bar{p} = \frac{p}{c_{55}H} \\ &\bar{\rho} = 1;\ \bar{\omega} = \frac{\omega H}{c_s};\ \bar{t} = \frac{t c_s}{H};\ c_s := \sqrt{\frac{c_{55}}{\rho}};\ \bar{c}_s := 1 \end{aligned} \tag{1}$$

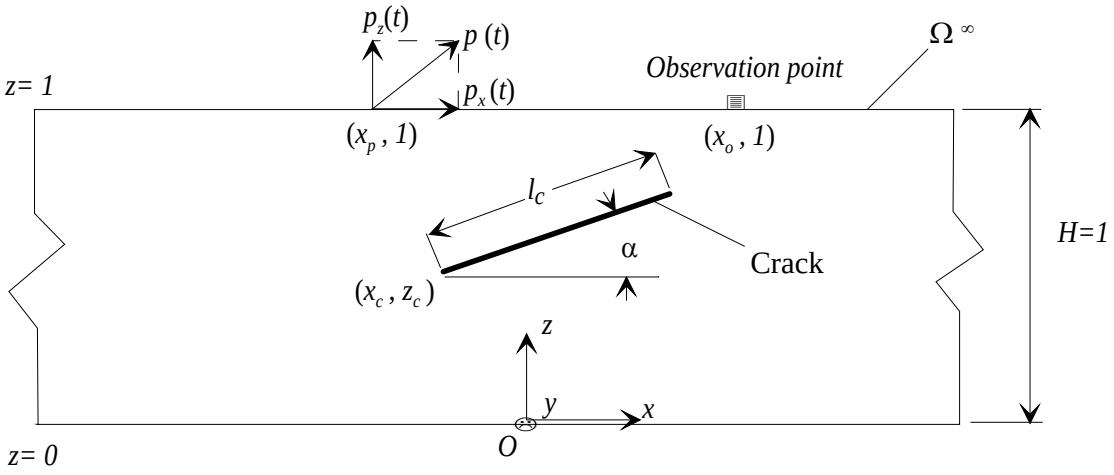

Figure 1: A schematic of an infinite, cracked plate subject to a line load

The over-bar, denoting dimensionless quantities, will be omitted in subsequent equations for notational convenience. In this paper we seek the replacement of the infinite domain, Ω^∞, with a truncated domain, Ω and two PMLs, Ω^P, at $x = \pm l$, see Fig. 2. As a result of the above replacement, we obtained a combined computational domain, $\Omega^c = \Omega \cup \Omega^P$. Steady-state, P-SV wave motion of the infinite plate in Fig. 1, is governed by the following displacement-based equilibrium equation [13]:

$$\begin{aligned} &\boldsymbol{c}_{xx}\boldsymbol{v}_{,xx} + \boldsymbol{c}_{xz}\boldsymbol{v}_{,xz} + \boldsymbol{c}_{xz}^T\boldsymbol{v}_{,zx} + \boldsymbol{c}_{zz}\boldsymbol{v}_{,zz} + \omega^2\boldsymbol{v} = \boldsymbol{0} \\ &\boldsymbol{v} = \{u \quad w\}^T, \ \boldsymbol{c}_{ij} = \boldsymbol{I}_i^T \boldsymbol{c} \boldsymbol{I}_j, \ \text{i,j=}x, z \\ &\boldsymbol{c} = \begin{bmatrix} c_{11} & c_{12} & 0 \\ c_{12} & c_{22} & 0 \\ 0 & 0 & c_{55} \end{bmatrix}, \ \boldsymbol{I}_x = \begin{bmatrix} 1 & 0 \\ 0 & 0 \\ 0 & 1 \end{bmatrix}, \ \boldsymbol{I}_z = \begin{bmatrix} 0 & 0 \\ 0 & 1 \\ 1 & 0 \end{bmatrix} \end{aligned} \tag{2}$$

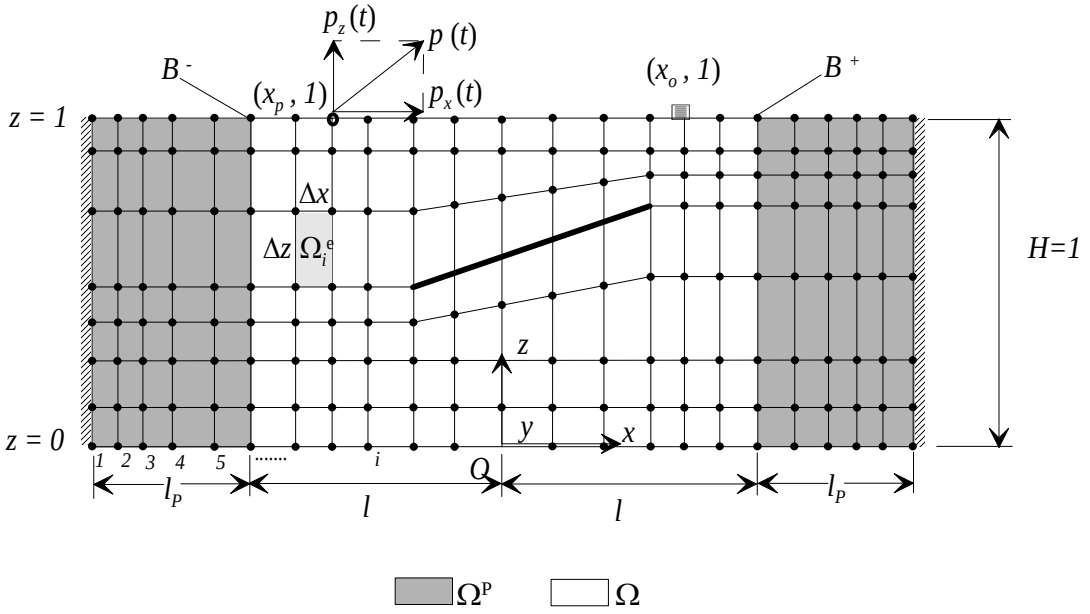

Figure 2: A schematic of the FE-PML model of the infinite plate in Fig. 1

Computational representation of this infinite plate with an FE-PML model as shown in Fig. 2, requires the replacement of x by a stretched coordinate, $\tilde{x}$, defined in terms of a real damping profile, ζ, and frequency, ω, as described in [9]:

$$\tilde{x}(x) := \begin{cases} x & |x| \le l \\ l + \dfrac{1}{j\omega}\displaystyle\int_{s=l}^{s=x} \zeta(s)\,ds & |x| > l, \end{cases} \tag{3}$$

Thus, frequency-domain equilibrium equation of the FE-PML model can be written as:

$$\boldsymbol{c}_{xx}\boldsymbol{v}_{,\tilde{x}\tilde{x}} + \boldsymbol{c}_{xz}\boldsymbol{v}_{,\tilde{x}z} + \boldsymbol{c}_{xz}^{T}\boldsymbol{v}_{,z\tilde{x}} + \boldsymbol{c}_{zz}\boldsymbol{v}_{,zz} + \omega^2\boldsymbol{v} = \boldsymbol{0} \tag{4}$$

Using the chain rule to expand the first three differential terms on the left hand side of Eq. (4) followed by the evaluation of $x_{,\tilde{x}}$ and $x_{,\tilde{x}\tilde{x}}$ from Eq. (3) using the continuity of the damping profile, ζ, results in

$$\begin{aligned} \frac{\boldsymbol{c}_{xx}}{\left[j\omega+\zeta\right]^2}\boldsymbol{v}_{,xx} - \frac{\zeta_{,x}\,\boldsymbol{c}_{xx}}{\left[j\omega+\zeta\right]^3}\boldsymbol{v}_{,x} + \frac{\boldsymbol{c}_{xz}}{j\omega\left[j\omega+\zeta\right]}\boldsymbol{v}_{,xz} \\ + \frac{\boldsymbol{c}_{xz}^{T}}{j\omega\left[j\omega+\zeta\right]}\boldsymbol{v}_{,zx} - \frac{\boldsymbol{c}_{zz}}{\omega^2}\boldsymbol{v}_{,zz} = \boldsymbol{v}. \end{aligned} \tag{5}$$

By splitting displacement wave-field [6], Eq. (5) can be written as

$$\boldsymbol{v} = \boldsymbol{v}_1 + \boldsymbol{v}_2 + \boldsymbol{v}_3 + \boldsymbol{v}_4, \quad \boldsymbol{v}_i = \begin{Bmatrix} u_i & w_i \end{Bmatrix}^T \quad i = 1,...,4 \tag{6a}$$

$$\boldsymbol{c}_{xx}\boldsymbol{v}_{,xx} = \left[j\omega+\zeta\right]^2\boldsymbol{v}_1, \tag{6b}$$

$$-\boldsymbol{\zeta}_{,x}\,\boldsymbol{c}_{,xx}\boldsymbol{v}_{,x} = \left[j\omega+\boldsymbol{\zeta}\right]^3\boldsymbol{v}_2, \tag{6c}$$

$$\boldsymbol{c}_{xz}\boldsymbol{v}_{,xz} + \boldsymbol{c}_{xz}^{T}\boldsymbol{v}_{,zx} = j\omega\left[j\omega+\zeta\right]\boldsymbol{v}_3, \tag{6d}$$

$$\boldsymbol{c}_{zz}\boldsymbol{v}_{,zz} = -\omega^2\boldsymbol{v}_4 \tag{6e}$$

Inverse Fourier transformation of Equations (6b) through (6e) yields the following displacement-based governing equations in the time domain

$$\ddot{\tilde{\boldsymbol{v}}}_1 = \boldsymbol{c}_{xx}\boldsymbol{v}_{,xx} : \quad \ddot{\tilde{\boldsymbol{v}}}_1 = \left(\partial_t + \boldsymbol{\zeta}\right)^2\boldsymbol{v}_1 \tag{7a}$$

$$\ddot{\tilde{\boldsymbol{v}}}_5 = -\boldsymbol{\zeta}_{,x}\;\boldsymbol{c}_{xx}\;\boldsymbol{v}_{,x}, \tag{7b}$$

$$\boldsymbol{v}_5 = \dot{\tilde{\boldsymbol{v}}}_2, \tag{7c}$$

$$\boldsymbol{c}_{xz}\boldsymbol{v}_{,xz} + \boldsymbol{c}_{xz}^{T}\boldsymbol{v}_{,zx} = \dot{\tilde{\boldsymbol{v}}}_3, \; \dot{\tilde{\boldsymbol{v}}}_3 = \partial_t\left(\partial_t + \zeta\right)\boldsymbol{v}_3 \tag{7d}$$

$$\boldsymbol{c}_{zz}\boldsymbol{v}_{,zz} = \ddot{\boldsymbol{v}}_4 \tag{7e}$$

Note that Equation (6c), which has a third-order time derivative, is split now into Equations (7b) and (7c) that involves only second- and first-order time derivatives, respectively. In a standard finite element procedure, the entire problem domain is divided into a finite number, n_e, of non-overlapping elements, Ω_i^e $(i = 1...n_e)$. Approximations to the solutions of Eq. (7a, b, d, and e) are expressed over each element in terms of element nodal values and piecewise-continuous, linearly-

independent basis functions, N^{j} $(j=1...n_n^e)$ with n_n^e being the number of nodes in an element. Following a Galerkin method in eliminating the integral of the weighted approximation residuals over the entire problem domain, where basis functions are used as weights, results in the following finite element form of Eq. (7)

$$\boldsymbol{q}=\boldsymbol{q}_1+\boldsymbol{q}_2+\boldsymbol{q}_3+\boldsymbol{q}_4,$$

$$\boldsymbol{q}=\left\{u^1 \quad w^1 \quad ... \quad u^{n_n} \quad w^{n_n}\right\} \tag{8a}$$

$$\boldsymbol{q}_i=\left\{u_i^1 \quad w_i^1 \quad ... \quad u_i^{n_n} \quad w_i^{n_n}\right\},\ i=1...4$$

$$\boldsymbol{M}\ddot{\tilde{\boldsymbol{q}}}_1=\boldsymbol{P}-\boldsymbol{K}_1\boldsymbol{q}, \tag{8b}$$

$$\boldsymbol{M}\ddot{\tilde{\boldsymbol{q}}}_5=-\boldsymbol{K}_2\boldsymbol{q}, \tag{8c}$$

$$\boldsymbol{q}_5=\dot{\tilde{\boldsymbol{q}}}_2, \tag{8d}$$

$$\boldsymbol{M}\dot{\tilde{\boldsymbol{q}}}_3=-\boldsymbol{K}_3\boldsymbol{q}. \tag{8e}$$

$$\boldsymbol{M}\ddot{\boldsymbol{q}}^4=-\boldsymbol{K}_4\boldsymbol{q}. \tag{8f}$$

In Eq. (8a), n_n is the number of global nodes in the finite element mesh. The mass matrix, $\boldsymbol{M}$, stiffness matrices, $\boldsymbol{K}_i$ $(i=1...4)$, and consistent load vector, $\boldsymbol{P}$, are obtained by standard finite element assembly, denoted by Π, of the corresponding element-level matrices as follows:

$$\boldsymbol{K}_1=\prod_{i=1}^{i=n_e}\left\{\sum_k^{n_n^e}\sum_{j=1}^{n_n^e}\int_{\Omega_i^e}N^k_{,x}\boldsymbol{c}'_{xx}N^j_{,x}dxdz\right\}, \tag{9a}$$

$$\boldsymbol{K}_2=\prod_{i=1}^{i=n_e}\left\{\sum_k^{n_n^e}\sum_{j=1}^{n_n^e}\int_{\Omega_i^e}N^k\zeta_{,x}\boldsymbol{c}'_{xx}N^j_{,x}dxdz\right\}, \tag{9b}$$

$$\boldsymbol{K}_3=\prod_{i=1}^{i=n_e}\left\{\sum_{k=1}^{n_n^e}\sum_{j=1}^{n_n^e}\int_{\Omega_i^e}\left[N^k_{,x}\boldsymbol{c}'_{xz}N^j_{,z}+N^k_{,z}\boldsymbol{c}'_{xz}N^j_{,x}\right]dxdz\right\}, \tag{9c}$$

$$\boldsymbol{K}_4=\prod_{i=1}^{i=n_e}\left\{\sum_{k=1}^{n_n^e}\sum_{j=1}^{n_n^e}\int_{\Omega_i^e}N^k_{,z}\boldsymbol{c}'_{zz}N^j_{,z}dxdz\right\}, \tag{9d}$$

$$\boldsymbol{P}=\prod_{i=1}^{i=n_e}\left\{\sum_{k=1}^{n_n^e}\sum_{j=1}^{n_n^e}\int_{\Omega_i^e}N^k\boldsymbol{I}\ p\delta\left(x_p\right)dx\right\}, \tag{9e}$$

$$\boldsymbol{M}=\prod_{i=1}^{i=n_e}\left\{\sum_{k=1}^{n_n^e}\sum_{j=1}^{n_n^e}\int_{\Omega_i^e}N^k\boldsymbol{I}\ N^j dxdz\right\}. \tag{9f}$$

$$\boldsymbol{c}'_{ij}=\boldsymbol{I}\boldsymbol{c}_{ij}\boldsymbol{I};\ \boldsymbol{I}=\begin{bmatrix}1 & 0\\ 0 & 1\end{bmatrix};\ i,j=x,z \tag{9g}$$

Inside Ω, standard finite element equations corresponding to (2) can be integrated using a Newmark explicit scheme. Inside Ω^P, Eqs. (8b, c, d, e, and f) can be integrated in the followings steps:

$$\ddot{\boldsymbol{q}}_{1(i+1)} = \frac{\boldsymbol{M}^{-1}\left[\boldsymbol{P}_x - \boldsymbol{K}_1\boldsymbol{q}\right] - \zeta\left\{\zeta\boldsymbol{q}_{1(i)} + \left[1+\frac{\zeta\Delta t}{2}\right]\left[\ddot{\boldsymbol{q}}_{1(i)}\Delta t + 2\dot{\boldsymbol{q}}_{1(i)}\right]\right\}}{\left[1+\zeta\Delta t+\left(\zeta\Delta t\right)^2\right]},$$

$$\dot{\boldsymbol{q}}_{1(i+1)} = \dot{\boldsymbol{q}}_{1(i)} + \frac{\ddot{\boldsymbol{q}}_{1(i)} + \ddot{\boldsymbol{q}}_{1(i+1)}}{2}\Delta t, \tag{10a}$$

$$\boldsymbol{q}_{1(i+1)} = \boldsymbol{q}_{1(i)} + \left(\dot{\boldsymbol{q}}_{1(i+1)} + \frac{\ddot{\boldsymbol{q}}_{1(i+1)}}{2}\Delta t\right)\Delta t$$

$$\ddot{\boldsymbol{q}}_{5(i+1)} = \frac{-\boldsymbol{M}^{-1}\boldsymbol{K}_1\boldsymbol{q} - \zeta\left\{\zeta\boldsymbol{q}_{5(i)} + \left[1+\frac{\zeta\Delta t}{2}\right]\left[\ddot{\boldsymbol{q}}_{5(i)}\Delta t + 2\dot{\boldsymbol{q}}_{5(i)}\right]\right\}}{\left[1+\zeta\Delta t+\left(\zeta\Delta t\right)^2\right]},$$

$$\dot{\boldsymbol{q}}_{5(i+1)} = \dot{\boldsymbol{q}}_{5(i)} + \frac{\ddot{\boldsymbol{q}}_{5(i)} + \ddot{\boldsymbol{q}}_{5(i+1)}}{2}\Delta t, \tag{10b}$$

$$\boldsymbol{q}_{5(i+1)} = \boldsymbol{q}_{5(i)} + \left(\dot{\boldsymbol{q}}_{5(i+1)} + \frac{\ddot{\boldsymbol{q}}_{5(i+1)}}{2}\Delta t\right)\Delta t$$

$$\boldsymbol{q}_{2(i+1)} = \frac{\left(\boldsymbol{q}_{2(i)} + \boldsymbol{q}_{5(i+1)}\Delta t\right)}{\left(1+\zeta\Delta t\right)} \tag{10c}$$

$$\ddot{\boldsymbol{q}}_{3(i+1)} = \frac{-\boldsymbol{M}^{-1}\boldsymbol{K}_3\boldsymbol{q} - \zeta\dot{\boldsymbol{q}}_{3(i)} - \frac{\zeta\ddot{\boldsymbol{q}}_{3(i)}}{2}\Delta t}{\left[1+\frac{\zeta\Delta t}{2}\right]},$$

$$\dot{\boldsymbol{q}}_{3(i+1)} = \dot{\boldsymbol{q}}_{3(i)} + \frac{\ddot{\boldsymbol{q}}_{3(i)} + \ddot{\boldsymbol{q}}_{3(i+1)}}{2}\Delta t, \tag{10d}$$

$$\boldsymbol{q}_{3(i+1)} = \boldsymbol{q}_{3(i)} + \left(\dot{\boldsymbol{q}}_{3(i+1)} + \frac{\ddot{\boldsymbol{q}}_{3(i+1)}}{2}\Delta t\right)\Delta t$$

$$\ddot{\boldsymbol{q}}_{4(i+1)} = -\boldsymbol{M}^{-1}\boldsymbol{K}_4\boldsymbol{q},$$

$$\dot{\boldsymbol{q}}_{4(i+1)} = \dot{\boldsymbol{q}}_{4(i)} + \frac{\ddot{\boldsymbol{q}}_{4(i)} + \ddot{\boldsymbol{q}}_{4(i+1)}}{2}\Delta t, \tag{10e}$$

$$\boldsymbol{q}_{4(i+1)} = \boldsymbol{q}_{4(i)} + \left(\dot{\boldsymbol{q}}_{4(i+1)} + \frac{\ddot{\boldsymbol{q}}_{4(i+1)}}{2}\Delta t\right)\Delta t$$

An over-dot indicates a time derivative (velocity). Integration time step is Δt. Subscripts i and $i+1$ denote consecutive time steps. The FE-PML model was programmed into a FORTRAN 90 computer code. The code was executed on a Dell Precision M6300 for several example problems. Results are presented and discussed next.

3 Numerical implementation and validation

Accuracy and stability of FE modeling of elastic wave motion is dependent on element dimensions, Δx and Δy. Several recommendations [e.g. 14] suggest a minimum of eight linear or four quadratic elements per shortest wave length in order to correctly capture a waveform. We will refer to this later as the eight-element rule. Moreover, stability of explicit time integration is critically dependent on time step, Δt. A stable time step is given in terms of element dimensions, Δx and Δy, and pressure wave speed, c_p, as follows [e.g. 15]

$$\Delta t \leq \frac{1}{c_p}\left(1/\Delta x^2 + 1/\Delta y^2\right)^{-1/2} \tag{11}$$

Basu [11] has found a stable time step for an FE model to remain stable in an FE-PML model. The real damping profile in the PML region assumes the following form [9]:

$$\zeta(x) = \zeta_0 \left(\frac{x-l}{l_p}\right)^m \tag{12}$$

ζ_0 is a real number and m is an integer exponent. A discussion of the effect of these parameters on PML performance is available in the literature [e.g. 9]. In all numerical examples throughout this paper, ζ and m are kept at 10 and 1, respectively.

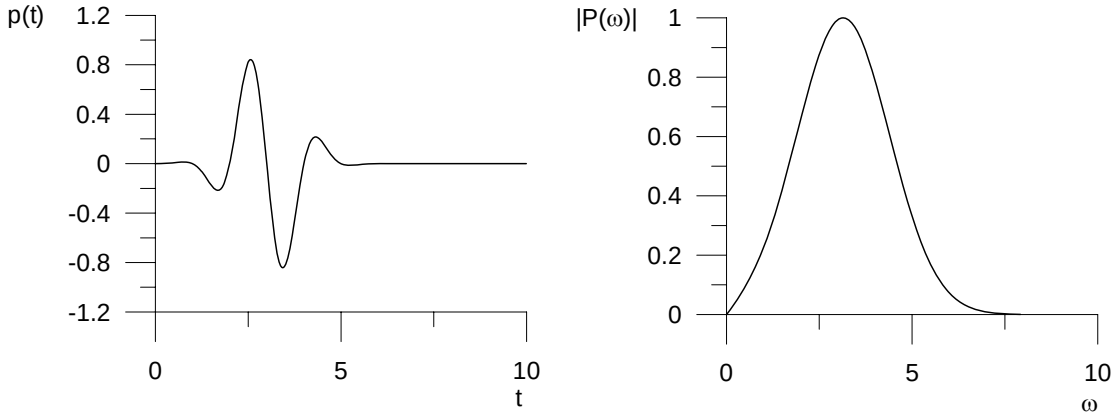

(a) (b)

Figure 3: A modulated Gaussian signal (a) time history and (b) frequency spectrum

In the following, numerical results are presented to verify reciprocity satisfaction of FE and FE-PML predictions and to establish their validity against available literature data. Time history responses are predicted at $(5,1)$ due to a loading at $(-5,1)$ in the form of a modulated Gaussian signal whose time history is given by:

$$p(t) = \frac{2}{\sigma\sqrt{2\pi}} \exp\left[-\frac{(t-t_0)}{2\sigma^2}\right] \sin(\omega_c t), \tag{13}$$

In Eq. (13), σ is a parameter controlling the width of the pulse, t_0 determines the time delay, and ω_c is the center angular frequency. In this example, $\sigma = 0.8$, $t_0 = 3$, $\omega_c =$

3.14 are chosen. Time history and frequency spectrum of a Gaussian signal corresponding to these values are shown in Fig. 3.

Two sets of predictions were reported in the literature for this loading-observation scenario. The first was reported by Pan and Datta [16] for a $100\mu m$-thick , nickel layer whose dimensional properties were given as $c_{11} = c_{22} = 298.95$ GPa , $c_{12} = 129.53$ GPa, $c_{55} = 84.71$ GPa , and $\rho = 8910$ kg/m^3. The second was reported by Liu and Achenbach [17] for an aluminum plate whose Poisson's ratio is $1/3$. Pan and Datta obtained their predictions analytically. Liu and Achenbach employed a Strip-Element Method (SEM) and corroborated their results with those of a Hybrid Numerical Method (HNM). Dimensionless frequency spectra of the nickel and aluminum plates are shown in Fig. 4, the two are nearly identical.

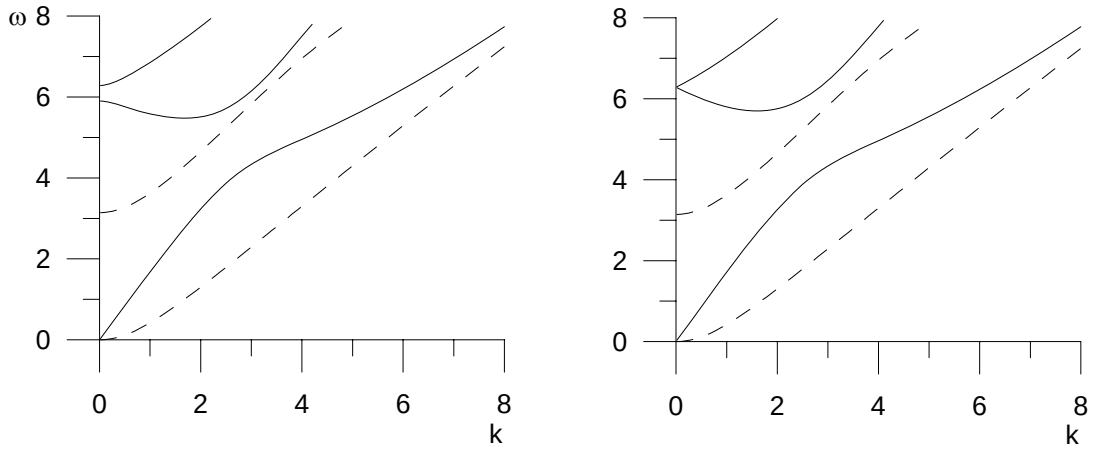

Figure 4: Frequency spectra for (a) the nickel layer and (b) aluminum plate (____ symmetric modes; ------- anti-symmetric modes)

Frequency band upper limit of the exciting signal at $\omega = 7$, see Fig. 3b, corresponds a maximum wavenumber $k = 8$ for both plates, see Fig. 4, i.e. a minimum wavelength $(\lambda = 2\pi/k)$ of about 0.8. Following the eight-element rule and Eq. (11), a uniform finite-element mesh of 0.1-by-0.1 elements and a time step of 0.03 are employed to obtain the results presented in this section.

Reciprocity is verified for the FE $(l = 15)$ and FE-PML $(l = 5.1; l_p = 1.9)$ models by predicting vertical, top-surface displacement at $(5,1)$ due to a vertical point load at $(-5,1)$ and vice versa. Two sets of such predictions for the nickel and aluminum plates are shown in Figs. 5 and 6. They are so indistinguishable that reciprocity is evidently satisfied.

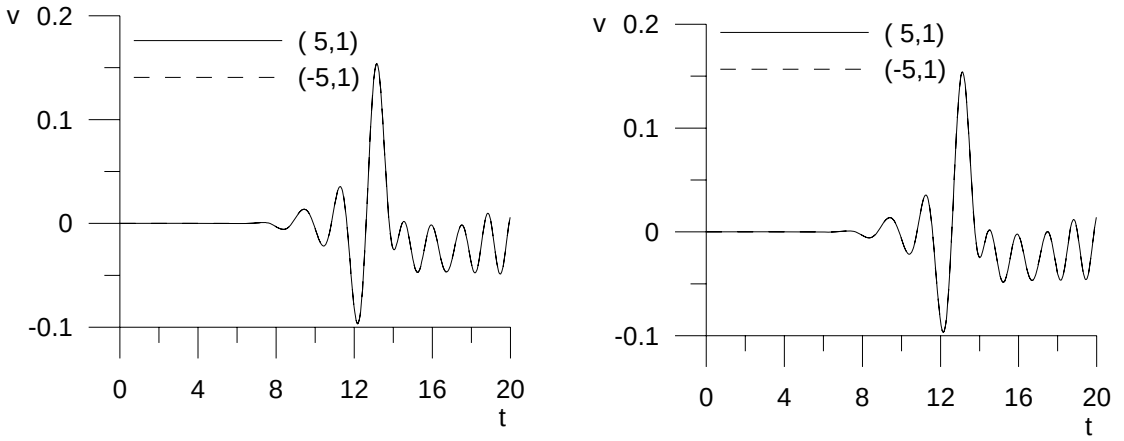

(a) (b)

Figure 5: Reciprocity check of (a) FE and (b) FE-PML predictions in the nickel layer

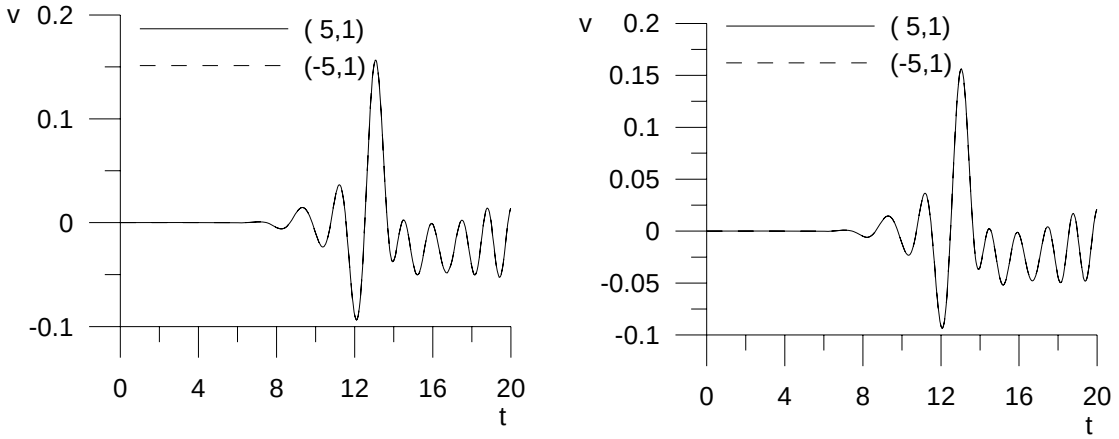

(a) (b)

Figure 6: Reciprocity check of (a) FE and (b) FE-PML predictions in the aluminum plate

Figure 7a shows horizontal top-surface displacement at $(5,1)$ in the nickel layer due to a horizontal load at $(-5,1)$. Both FE and FE-PML results are in good agreement with corresponding analytical predictions reported by Pan and Datta. Figure 7b depicts horizontal top-surface displacement at $(5,1)$ in the aluminum plate due to a horizontal load at $(-5,1)$. Similarly, FE and FE-PML predictions are in decent agreement with its counterparts reported by Liu and Achenbach. The CPU times elapsed during the FE (3000 elements) and the FE-PML (1400 elements) runs were: 772 and 498.2 seconds, respectively, saving 35.5 % of CPU time using the latter.

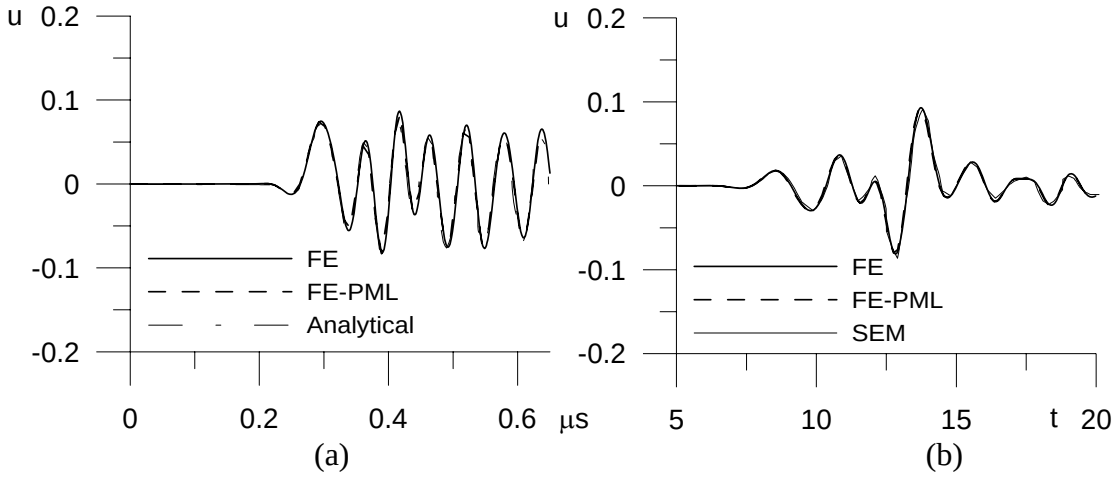

Figure 7: Horizontal top-surface displacements at $(5,1)$ due to (a) a horizontal load at $(-5,1)$ in the nickel layer and (b) a vertical load at $(-5,1)$ in the aluminum plate.

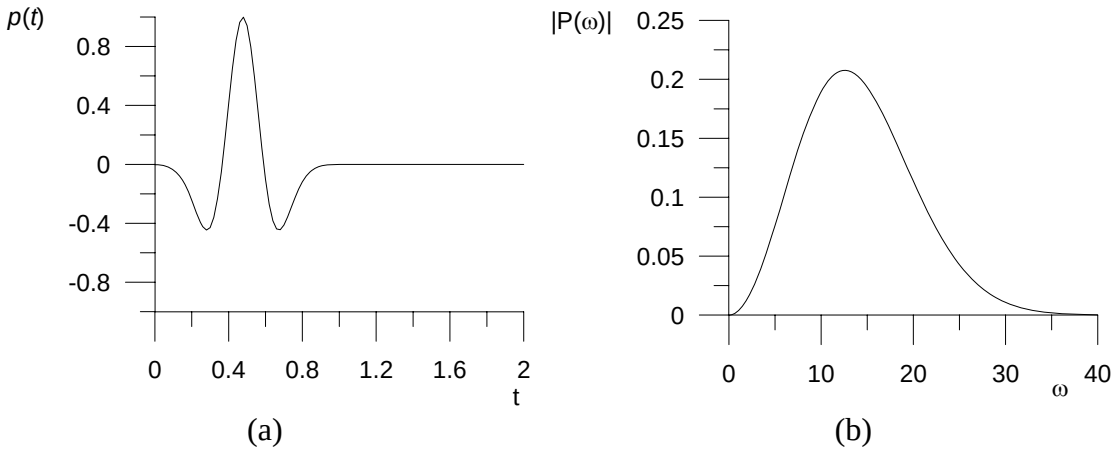

Figure 8: A Ricker wavelet (a) time history and (b) frequency spectrum for Example 1.

4 Applications to crack characterization

The following numerical examples demonstrate some applications of the proposed FE-PML model to numerical modeling of elastic P-SV wave scattering in the context of 2D crack characterization.

Example 1: A vertically cracked, 175-*mm* thick isotropic concrete slap is considered in this example. The vertical crack opens to the bottom surface of the slab. The crack tip lies at $x_c = (0, 0.5)$, i.e. $l_c = 0.5$. Density and Poisson's ratio of concrete are 2500 kg/m^3 and 0.15, respectively. The slab is excited by a Ricker wavelet in the form:

$$p(t) = \left[1 - 2\alpha\tau\right]\exp[-\alpha\tau]:\ \alpha = \pi^2\omega_c^2,\ \tau = \left(t - \frac{3\pi}{\omega_c}\right) \tag{13}$$

Time history and Fourier transform of a Ricker wavelet corresponding to $\omega_c = 2$ is shown in Fig. 8. Figure 9a shows frequency spectra for the concrete slab in this example. At the maximum significant frequency present in the exciting impact $\omega \approx 25$, see Fig. 7b, the wavenumber is, approximately, 14. That corresponds to a wavelength of 0.45. Following the eight-element rule and Eq. (11), a uniform mesh $(\Delta x = \Delta y = 0.05)$ and a time step of 0.008 are employed in the current example. Convergence of the FE-PML predictions of vertical top-surface displacement at $(0.12,1)$ due to a point load at $(-0.12,1)$ for this discretization values is confirmed by comparing the results for $\Delta x = \Delta y = 0.05$ and 0.04, see Fig. 10b.

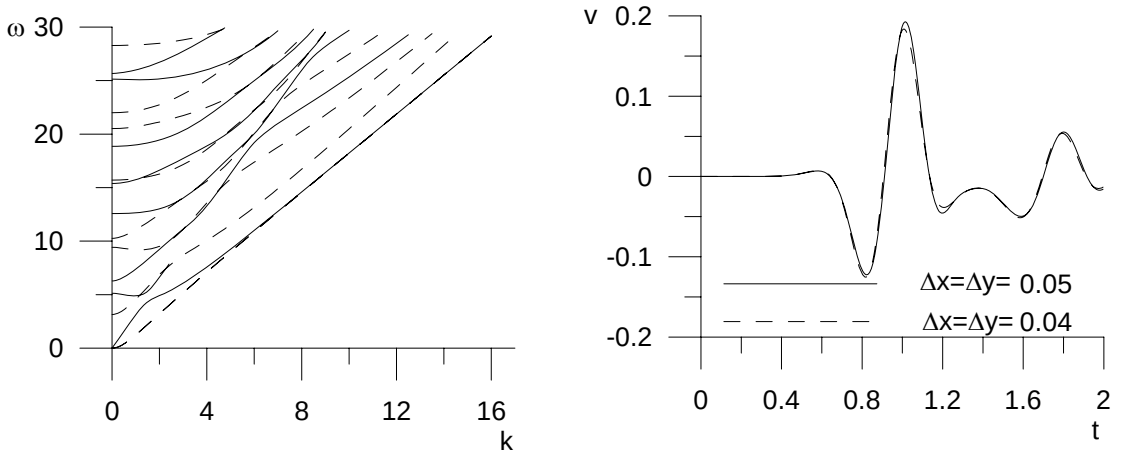

(a) (b)

Figure 9: (a) Frequency spectra in the concrete slab; (b) vertical top-surface displacement at $(0.12,1)$ due to a point load at $(-0.12,1)$ is nearly invariant to further mesh refinement.

Predictions of displacement time histories in response to a vertical load are obtained by FEA with PMLs $(l = 1,\ l_p = 1)$ and without PML $(l = 5)$. Displacement time history responses at $x_o = (0.2,1)$ to a vertical line load at $x_p = (-0.2,1)$ are shown in Fig. 8, with very good agreement between the FE and the FE-PML predictions. It took the FE (8000 elements) and the FE-PML (1600 elements) executions 807.79 and 333.84 seconds of CPU time, respectively. That is a 58.7 % saving in CPU time. Obviously, a relatively larger FE model dictated by excitation of high-frequency content and a smaller FE-PML model due to load-observation closeness resulted in a higher saving in CPU time. Thus, FE-PML can allow a comprehensive study of the effect of crack presence on response time histories and/or frequency spectra at a reasonable computational cost.

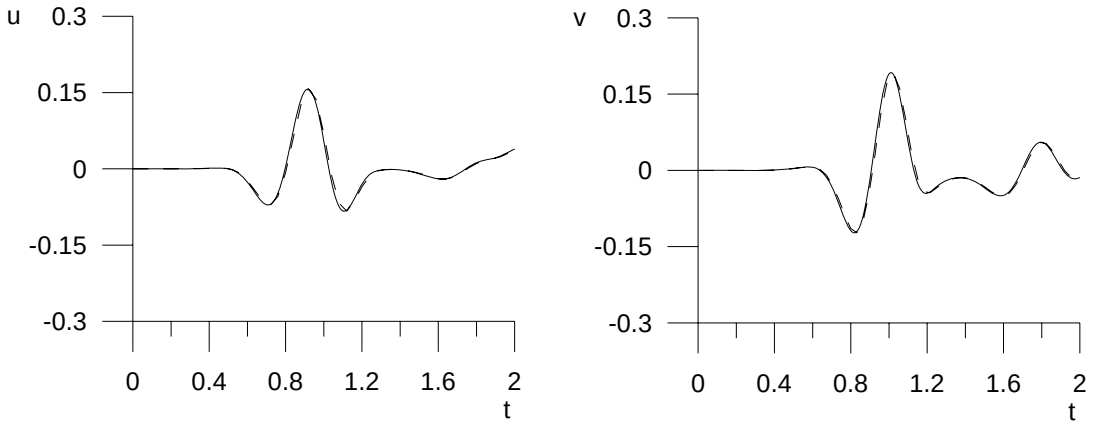

Figure 10: (a) Horizontal and (b) vertical displacement time-histories at $x_0 = (0.2,1)$ due to a line load at $x_p = (-0.2,1)$ in the flawless concrete slab predicted by FE (dashed) and FE-PML (solid)

Let us consider another loading-observation scenario. A vertical line load is applied to the bottom surface of the slab at $x_p = -0.1$. Slab's bottom surface, vertical displacement time history is predicted at $x_o = 0.1$ by the FE-PML model for several values of crack length, l_c. Predictions are shown in Fig. 11a. The effect of crack length on time of arrival, T, is evident. Figure 11b is a plot of arrival time, T, versus crack length, l_c. The relationship between T and l_c is tri-linear. Arrival time is insensitive to crack lengths less than or equal to 0.1. For crack lengths between 0.1 and 0.7, time of arrival increases with crack length at a constant rate. This rate increases at $l_c = 0.7$. This proportionality between the time delay of the transmitted wave and a crack's depth confirms what has been reported in literature [18].

Example 2: Let's consider a delaminated, 6.35-*mm* thick, 0^o (bottom)/90^o (top) graphite-epoxy laminate. Its configuration and material properties are given in Table 1. Results are obtained by FE with a PML ($l = 1.1, l_p = 0.9$) and without a PML ($l = 6$). From Fig. 12b and 13a, value of shortest wavelength was calculated to be 0.4. Following the eight-element rule and Eq. (11), a uniform 0.05-by-0.05 finite element mesh and time step of 0.005 are used in this example. Convergence for these discretization values is evident from Fig. 13b.

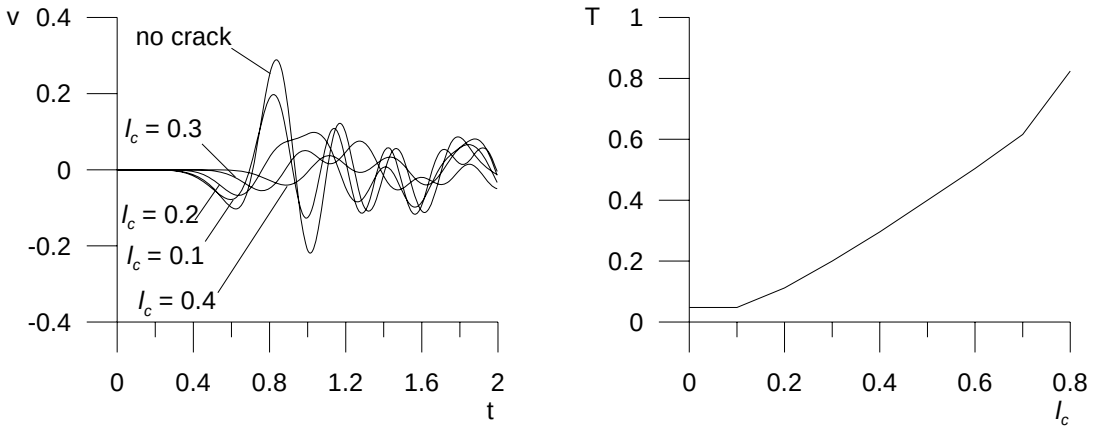

(a) (b)

Figure 11: (a) Vertical displacement time histories at (0.1,0) due to a vertical line load at $(-0.1, 0)$ for different values of crack length, l_c ; (b) corresponding arrival time, T , plotted versus crack length, l_c

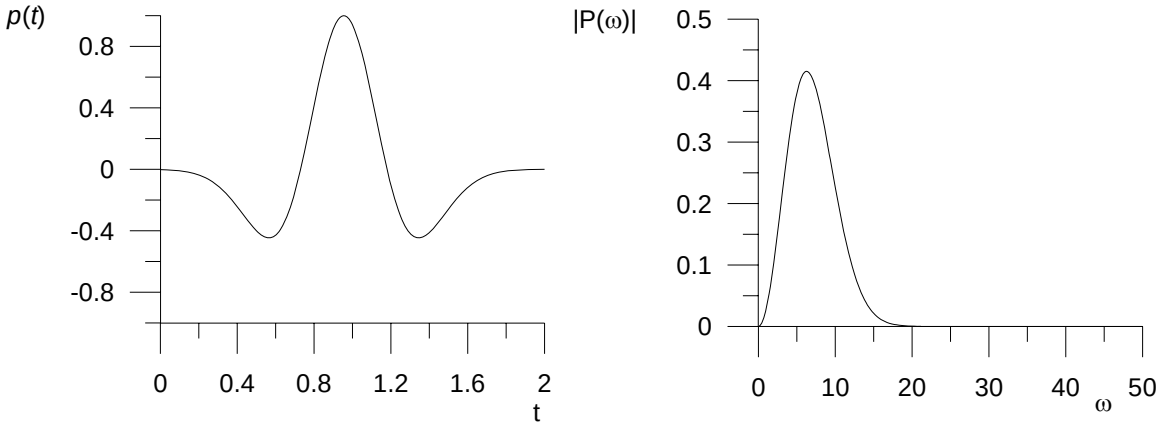

(a) (b)

Figure 12: A Ricker wavelet (a) time history and (b) frequency spectrum for Example 3.

Time histories of top-surface displacement at $x_o = 0.75$ due to a line load at $x_p = -0.75$ were predicted by FE (4800 elements) and FE-PML (1760 elements) models consuming 4299.94 seconds and 1985.96 seconds of CPU time, respectively, with 53.8 % saving in CPU time by using the latter. Results are in very good agreement as shown in Fig. 14. The FE-PML model was used to conduct a study of the effect of load-observation separation distance, *d*, on arrival time, *T*, of bottom-surface vertical displacement response due to a vertical line load applied to the top surface of the laminate. Four load-observation configurations considered in this study are summarized in Table 2 and illustrated in Fig. 14.

Table 1: Material and configuration of the graphite-epoxy laminate in Example 3

Lamina	H	ρ	C_{11}	c_{12}	c_{22}	c_{55}
	Mm	10^3kg/m^3	Gpa	GPa	GPa	GPa
0^o	3.175	1.578	160.72	6.43	13.91	7.07
90^o	3.175	1.578	13.91	6.91	13.91	3.49

Figure 16a shows the time of arrival, *T*, versus crack length for the four configurations. It is evident that the closer the observation point is to the load, the more distinct the change in time of arrival becomes. It is noticeable also that each curve exhibits a hump at a different value of crack length, l_c. Figure 16b shows variation in arrival time, *T*, with load-observation separation distance, *d*. As the separation distance increases, the time of arrival becomes insensitive to smaller crack lengths. This is a clear indication that a varying time of arrival, *T*, belongs, indeed, to a crack-tip diffracted wave not a transmitted one. Thus, for a fixed load-observation separation, there is a critical crack length below which the observation point is no longer inside the shadow zone of the crack. For configuration 1 and 2, these critical lengths are 0.8 and 0.4, respectively.

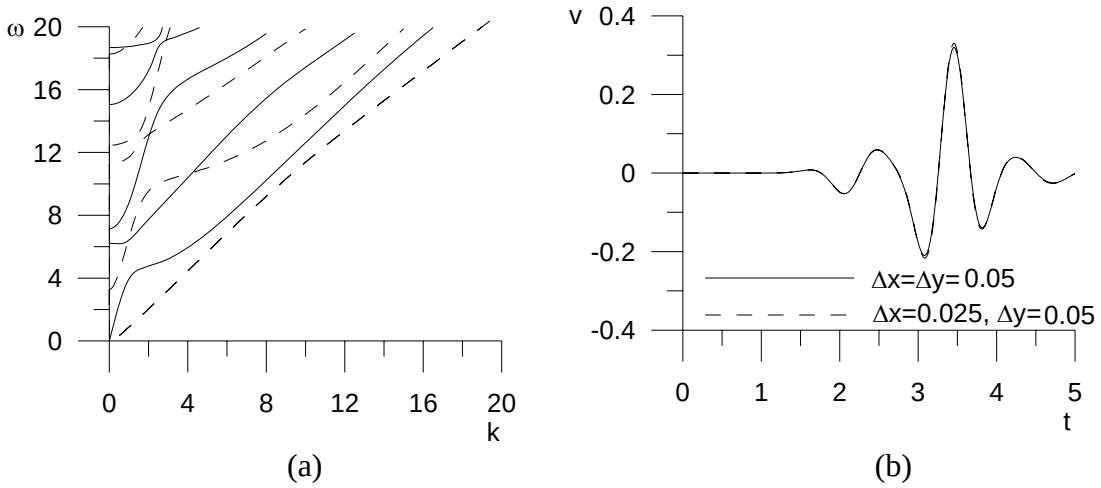

Figure 13: (a) Frequency spectra in the graphite-epoxy laminate; (b) vertical top-surface displacement at $(0.75,1)$ due to a point load at $(-0.75,1)$ is nearly invariant to further mesh refinement.

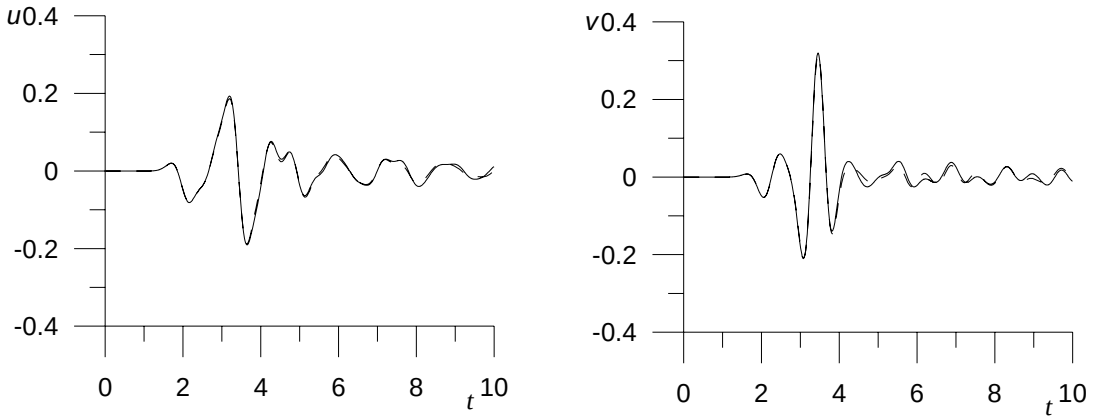

(a) (b)

Figure 14: Time histories at $x_o = 0.75$ of (a) horizontal and (b) vertical top-surface displacements predicted by FE (dashed line) and FE-PML (solid line)

Table 2: Load-configuration Configurations

Configuration	1	2	3	4
Load	(-0.75,1)	(-0.50,1)	(-0.25,1)	(0,1)
Observation	(0.75,0)	(0.50,0)	(0.25,0)	(0,0)
D	1.5	1	.5	0

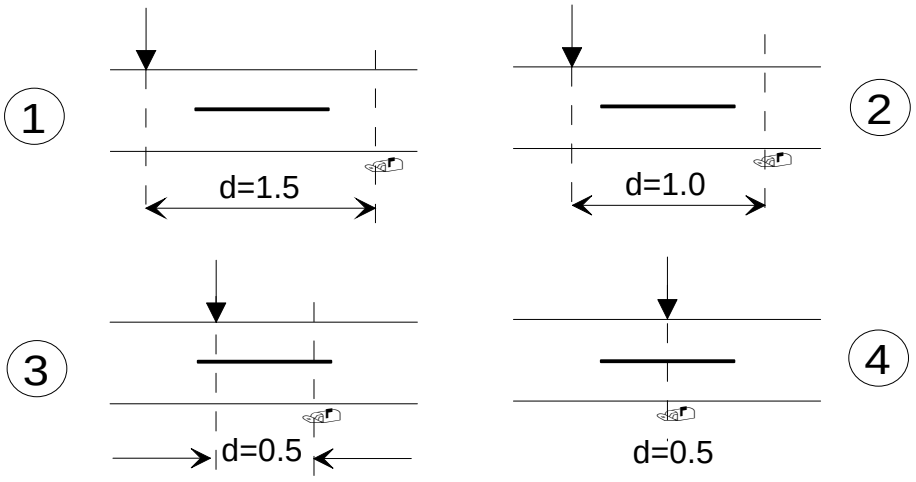

Figure 15: Illustrations of the configurations in Table 2.

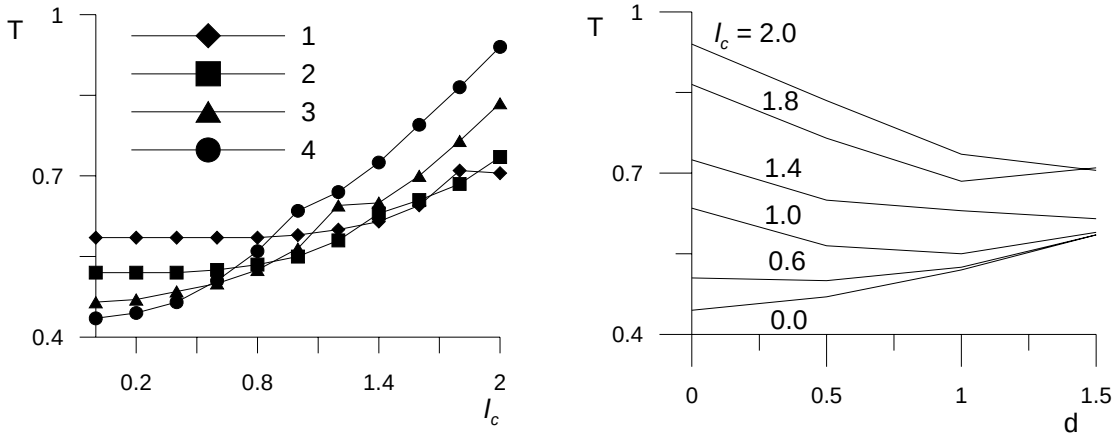

(a) (b)

Figure 16: (a) Variations in arrival time, *T*, with load-observation separation distance, *d*, for several delamination lengths (b) Variations in arrival time, T, with delamination length for several load-observation configurations.

5 Conclusions

This paper has successfully proven the applicability a combined, split-field PML and FE approach to numerical modeling of P-SV wave propagation and scattering in infinite plates. Results are in good agreement with available analytical and semi analytical solutions. The FE-PML offers an economical computational tool for analyzing elastic P-SV wave scattering problems in infinite plates. Saving in CPU times is application-dependent. For applications considered in this paper, these savings by the FE-PML model range between 29% and 87 % of the CPU time needed to run a corresponding FEA. Application of the proposed technique was used to study the correlation between the arrival time of crack-tip diffraction and crack depth or delamination length. Such studies are crucially helpful in setting experimental parameters or analyzing measured NDT data.

References

[1] J. P. Berenger, A perfectly matched layer for the absorption of electromagnetic waves, J. Comp. Phys., 114 (1994), 185-200.

[2] W. C. Chew and W. H. Weedon, A 3D perfectly matched medium from modified Maxwell's equations with stretched coordinates, Mic. Opt. Tech. Let. 7 (1994) 599-604.

[3] F. D. Hastings, J. B. Schneider and S. L. Broschat, Application of the perfectly matched layer (PML) absorbing boundary condition to elastic wave propagation, J. Acoust. Soc. Am. 100 (1996) 3061-3069.

[4] W. C. Chew and Q. H. Liu, Perfectly matched layers for elastodynamic: A new absorbing boundary condition, J. Comp. Acoust. 4 (1996) 341-359.

[5] Q. H. Liu, Perfectly matched layers for elastic waves in cylindrical coordinates, J. Acoust. Soc. Am. 105 (1999) 2075-2084.
[6] F. Collino and C. Tsogka, Application of perfectly matched absorbing layer model to the linear elastodynamic problem in anisotropic heterogeneous media, Geophysics 66 (2001) 294-307.
[7] F. Becache, P. Joly and C. Tsogka, Fictitious domains, mixed finite elements and perfectly matched layers for 2-D elastic wave propagation, J. Comp. Acoust. 3 (2001) 1175-1201.
[8] D. Komatitsch and J. Tromp, A perfectly matched layer absorbing boundary condition for the second-order seismic wave equation, Geophysics J. Int 154 (2003) 146-153.
[9] U. Basu and A. K. Chopra, Perfectly matched layers for time-harmonic elastodynamics of unbounded domains: theory and finite element implementation, Computer Meth. Appl. Mech. Eng. 192 (2003) 1337-1375.
[10] U. Basu and A. K. Chopra, Perfectly matched layers for transient elastodynamics of unbounded domains, Int. J. Num. Meth. Eng. 59 (2004) 1039-1074.
[11] U. Basu, Explicit finite element perfectly matched layer for transient three-dimensional elastic waves, Int. J. Num. Meth. Eng. 77 (2009) 151-176.
[12] W. C. Chew, J. M. Jin and E. Michieissen, Complex coordinate stretching as a generalized absorbing boundary condition, Microwave and Optical Technology Letters, 15 (1997) 363-369.
[13] E. Kausel, Fundamental Solutions in Elastodynamics: A Compendium, Cambridge University Press, 2006.
[14] G. R. Liu and Z. C. Xi, Elastic Waves in Anisotropic Laminates, CRC Press, Boca Raton, 2001.
[15] T. J. R. Hughes, Finite Element Method. Prentice-Hall, Englewood Cliffs, New Jersey, 1987.
[16] E. Pan and S. K. Datta, Ultrasonic waves in multilayered superconducting plates, J. App. Phys., 86 (1999) 543-551
[17] G. R. Liu and J. D. Achenbach, Strip element method to analyze wave scattering by cracks in anisotropic laminated plates, ASME J. App. Mech., 62 (1995) 607-613
[18] R. L. Hudgell, L. L. Morgan, R. F. Lumb, Non-destructive measurement of the depth of a surface-breaking cracks using ultrasonic Raleigh wave, Brit. J. NDT 16 (1974) 144-149

Received: June, 2009